NASA/TM-2003-212439
ARL-TR-3046

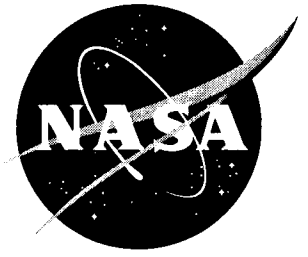

Characterization of Cracking and Crack Growth Properties of the C5A Aircraft Tie-Box Forging

Robert S. Piascik and Stephen W. Smith
Langley Research Center, Hampton, Virginia

John A. Newman
U.S. Army Research Laboratory
Vehicle Technology Directorate
Langley Research Center, Hampton, Virginia

Scott A. Willard
Lockheed Martin Engineering and Sciences
Langley Research Center, Hampton, Virginia

August 2003

The NASA STI Program Office . . . in Profile

Since its founding, NASA has been dedicated to the advancement of aeronautics and space science. The NASA Scientific and Technical Information (STI) Program Office plays a key part in helping NASA maintain this important role.

The NASA STI Program Office is operated by Langley Research Center, the lead center for NASA's scientific and technical information. The NASA STI Program Office provides access to the NASA STI Database, the largest collection of aeronautical and space science STI in the world. The Program Office is also NASA's institutional mechanism for disseminating the results of its research and development activities. These results are published by NASA in the NASA STI Report Series, which includes the following report types:

- TECHNICAL PUBLICATION. Reports of completed research or a major significant phase of research that present the results of NASA programs and include extensive data or theoretical analysis. Includes compilations of significant scientific and technical data and information deemed to be of continuing reference value. NASA counterpart of peer-reviewed formal professional papers, but having less stringent limitations on manuscript length and extent of graphic presentations.

- TECHNICAL MEMORANDUM. Scientific and technical findings that are preliminary or of specialized interest, e.g., quick release reports, working papers, and bibliographies that contain minimal annotation. Does not contain extensive analysis.

- CONTRACTOR REPORT. Scientific and technical findings by NASA-sponsored contractors and grantees.

- CONFERENCE PUBLICATION. Collected papers from scientific and technical conferences, symposia, seminars, or other meetings sponsored or co-sponsored by NASA.

- SPECIAL PUBLICATION. Scientific, technical, or historical information from NASA programs, projects, and missions, often concerned with subjects having substantial public interest.

- TECHNICAL TRANSLATION. English-language translations of foreign scientific and technical material pertinent to NASA's mission.

Specialized services that complement the STI Program Office's diverse offerings include creating custom thesauri, building customized databases, organizing and publishing research results ... even providing videos.

For more information about the NASA STI Program Office, see the following:

- Access the NASA STI Program Home Page at ***http://www.sti.nasa.gov***

- E-mail your question via the Internet to help@sti.nasa.gov

- Fax your question to the NASA STI Help Desk at (301) 621-0134

- Phone the NASA STI Help Desk at (301) 621-0390

- Write to:
  NASA STI Help Desk
  NASA Center for AeroSpace Information
  7121 Standard Drive
  Hanover, MD 21076-1320

NASA/TM-2003-212439
ARL-TR-3046

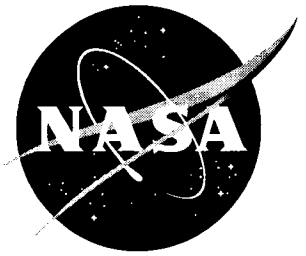

Characterization of Cracking and Crack Growth Properties of the C5A Aircraft Tie-Box Forging

Robert S. Piascik and Stephen W. Smith
Langley Research Center, Hampton, Virginia

John A. Newman
U.S. Army Research Laboratory
Vehicle Technology Directorate
Langley Research Center, Hampton, Virginia

Scott A. Willard
Lockheed Martin Engineering and Sciences
Langley Research Center, Hampton, Virginia

National Aeronautics and
Space Administration

Langley Research Center
Hampton, Virginia 23681-2199

August 2003

Available from:

NASA Center for AeroSpace Information (CASI)
7121 Standard Drive
Hanover, MD 21076-1320
(301) 621-0390

National Technical Information Service (NTIS)
5285 Port Royal Road
Springfield, VA 22161-2171
(703) 605-6000

Abstract

Detailed destructive examinations were conducted to characterize the integrity and material properties of two aluminum alloy (7075-T6) horizontal stabilizer tie box forgings removed from U.S. Air Force C5A and C5B transport aircraft. The C5B tie box forging was found to contain no evidence of cracking. Thirteen cracks were found in the C5A forging. All but one of the cracks observed in the C5A component were located along the top cap region (one crack was located in the bottom cap region). The cracks in the C5A component initiated at fastener holes and propagated along a highly tunneled intergranular crack path. The tunneled crack growth configuration is a likely result of surface compressive stress produced during peening of the forging surface. The tie box forging fatigue crack growth, fracture and stress corrosion cracking (SCC) properties were characterized. Reported herein are the results of laboratory air fatigue crack growth tests and 95% relative humidity SCC tests conducted using specimens machined from the C5A forging. SCC test results revealed that the C5A forging material was susceptible to intergranular environmental assisted cracking: the C5A forging material exhibited a SCC crack-tip stress-intensity factor threshold of less than 6 MPa$\sqrt{m}$. Fracture toughness tests revealed that the C5A forging material exhibited a fracture toughness that was 25% less than the C5B forging. The C5A forging exhibited rapid laboratory air fatigue crack growth rates having a threshold crack-tip stress-intensity factor range of <0.8 MPa$\sqrt{m}$. Detailed fractographic examinations revealed that the fatigue crack intergranular growth crack path was similar to the cracking observed in the C5A tie box forging. Because both fatigue crack propagation and SCC exhibit similar intergranular crack path behavior, the damage mechanism resulting in multi-site cracking of tie box forgings cannot be determined unless local cyclic stresses can be quantified.

Introduction

Nondestructive examinations (visual and eddy current) of the C5A horizontal stabilizer tie box forging shown in Figure 1 indicated the presence of through-the-thickness cracks emanating from fastener holes along the top and bottom cap regions. The subsequent inspection of a C5B aircraft conducted by the USAF revealed no evidence of cracking. Although both C5A and C5B tie box forgings are constructed of 7075T6 aluminum having the same nominal composition (1.6% Cu – 2.5% Mg – 5.6% Zn – 0.23% Cr, compositions in weight percent [1]), it was thought that differences in thermo-mechanical processing may have produced differences between the C5A and C5B material properties. A C5A and C5B tie box forging were sent from Robins AFB to NASA Langley Research Center for detailed destructive examination. The objective of this work was to:

(1) document the C5A forging cracking morphology,
(2) characterize the C5A stress corrosion cracking (SCC) properties,
(3) characterize the C5A forging fatigue crack growth properties,
(4) conduct detailed destructive examinations to determine if small insipient cracks were present (not detected be NDE) in the C5B forging, and
(5) characterize the fracture toughness properties of the C5A and C5B forgings.

Experimental Procedures

Destructive Examination

The location of all cracks was verified visually or by using the within-hole eddy current technique method. The cracks were carefully removed from the C5A component and examined using optical and scanning electron microscopy (SEM). Removal of the cracks from the forging was accomplished by cutting from the edge of the tie-box to the holes where the crack initiated and terminated. Two cracks were found to have initiated from a fastener hole and propagated without intersecting an adjacent hole. Here, one surface from each crack was carefully removed from the forging by cutting from the edge of the forging to the fastener hole, then placing a second saw cut close to the crack-tip and applying a small mode I load to fracture the remaining ligament between the crack-tip and the saw cut. Because no cracking was detected in the C5B forging by non-destructive examination (NDE), approximately thirty samples (fastener hole regions) were removed from the C5B forging in the regions that exhibited cracking in the C5A tie-box and examined for evidence of cracking by optical and scanning electron microscope (SEM) techniques. Here, the fastener hole was carefully bisected to expose the region of interest and each half was carefully strained open using a three-point-bend procedure. The three-point-bend straining technique was used to open insipient cracks that may have been present in the same orientation as noted in the C5A forging. Open cracks are easier to detect, so each strained specimen was examined for insipient cracks using the SEM.

Fatigue Crack Growth, Stress Corrosion Cracking, and Fracture Toughness Testing

Fracture toughness specimens machined from the C5A and C5B forgings and stress corrosion cracking (SCC) specimens machined from the C5A forging were obtained from the top cap center locations shown in Figure 2. The fatigue crack growth specimens were fabricated from the C5A top cap arm regions (Refer to Figure 1a). All specimens were machined from the forgings so that crack growth propagation was in the same orientation as the cracking observed in the C5A tie-box. Figure 3 is a schematic showing the compact tension (C(T)) specimen configurations used for fatigue crack growth and SCC tests. Fracture toughness tests were conducted using a wedge opening load (WOL) specimen described in Figure 3. Initial tests showed that a chevron notch configuration was required to ensure a uniform crack front shape during pre-cracking of the thicker (12.7 mm and 22.9 mm) specimen configurations.

The fatigue crack growth tests were performed under crack-tip stress-intensity factor (K) control using a computer-controlled closed-loop servo-hydraulic test machine. Specimens were loaded using a sinusoidal waveform at a frequency of 5 Hz in room temperature laboratory air. Low stress ratio ($R = 0.05$) and constant maximum stress-intensity factor ($K_{max} = 6.6$ and 13.2 MPa$\sqrt{m}$) tests were conducted in accordance with ASTM standard E 647 [2]. The $R = 0.05$ test was initiated at a cyclic stress-intensity factor (ΔK) of 5.5 MPa$\sqrt{m}$, and ΔK was decreased to characterize the cyclic stress-intensity factor threshold (ΔK_{th}) regime. An increasing ΔK test ($R = 0.05$) was performed on the same specimen to obtain the upper Paris regime ($\Delta K > 6$ MPa$\sqrt{m}$) fatigue crack growth characteristics.

The stress corrosion cracking tests were conducted in a plastic chamber where a >95% relative humidity environment was maintained by continually pumping moist air into the chamber. A temperature and humidity probe monitored the chamber environment. The SCC specimens were fatigue pre-cracked in laboratory air, and the SCC tests were conducted at constant load. The unloading compliance method was used to monitor crack length throughout the SCC tests; a back face strain gage was used to measure the change in specimen compliance per ASTM procedure [2]. Here, the load was decreased by a maximum of 25% to ensure that the crack wake remained open during the unloading compliance

measurements. After each test, an optical microscope was used to measure the crack surface length, and only small corrections (<5%) were made to the *in situ* compliance based crack length determinations. An average crack growth rate (d*a*/dt) and a corresponding averaged crack-tip stress-intensity factor (K) were calculated for each increment of crack growth.

The fracture toughness WOL specimens were fatigue pre-cracked in laboratory air to an approximate crack length of 30 mm. Fracture toughness testing was performed using a constant crosshead displacement rate resulting in a loading rate between 32 and 35 MPa$\sqrt{m}$/min, in accordance with ASTM standard E 399 [3]. Load and crack mouth opening data were obtained as each specimen was loaded. Following testing, the fatigue pre-crack was measured at multiple locations along the crack front per Section 8.2.2 of ASTM standard E 399 [3].

Results and Discussion

Destructive Examination Results

All C5A tie-box cracks found by NDE were carefully removed from the forging for detailed examination by optical and SEM microscopy. A total of thirteen cracks were examined; twelve cracks located along the top cap (center region and arm regions) and one crack located along the bottom cap (arm region). The dashed (dotted) line in Figure 4 shows the location of the crack between fastener holes #311 and #315. Analysis of the crack surface shown in Figure 5 revealed that the crack initiated along the interior of hole #311 and propagated approximately 3.2 cm (1-1/4 inch) to hole #315. The dark discolored region on the crack surface is a region of heavy corrosion products. The shape of the dark region indicates that the crack that propagated from hole #311 exhibited a highly curved crack front (tunneled crack front). The dashed lines in Figure 6 identify the location of cracks located between fastener holes #383, #385 and #387 and a long crack that propagated from hole #295. Analysis of the crack surface shown in Figure 7 reveals that a crack initiated at mid-thickness in fastener hole #383 and grew a length of approximately 4 cm (1.6 inch) through hole #385 and terminated in hole #387. The discolored regions on the crack surface shown in Figure 7 are associated with an accumulation of corrosion products. Following the region of crack initiation, a progression of crack fronts are identified by bands of discolored regions perpendicular to the direction of crack growth that suggest periods of crack arrest and subsequent propagation between holes #383 and #385. The crack front markings show that the crack propagated in a highly tunneled manner; it is important to note that the crack did not penetrate the forging surface until it had nearly propagated into the adjacent fastener hole #385. Faint colored crack arrest markings on the crack surface between hole #385 and hole #387 show that the crack likely reinitiated at the mid-thickness region in hole #385 and propagated towards hole #387 in a tunneled crack configuration. Figure 8 shows the crack surface of the 24 cm (9.5 inch) crack that initiated in the mid-thickness region of fastener hole #295. The distinct variations in color along the length of the crack surface are accumulated corrosion products and reveal the crack front configuration at various times during the life of the crack. These results show that severe crack tunneling occurred; after crack initiation, the tunneled crack propagated nearly 7.5 cm (3 inch) in the forging interior before the crack front had penetrated the surface of the forging. Both energy dispersive spectroscopy (EDS) and Auger analysis were performed to identify if chemical contaminants were associated with the crack surface corrosion products. No definitive contaminant was detected and no variation in chemical composition was linked to the dramatic variation in the surface corrosion along the length of the crack. These results suggest that crack environment (chemical composition) had not changed appreciably during crack growth and also suggests that the dramatic variation in crack surface discoloration is the result of corrosion product thickness and not corrosion product chemistry.

Figure 9 shows the location and orientation of the crack that initiated at fastener hole #276 in the tie-box lower cap arm. Figure 10 shows the surface of the crack; here, two halves (metallographic sections) of the specimen were placed together so the complete crack surface could be viewed. The crack initiated in the interior of fastener hole #276. The dashed line marks the curved crack front. The discolored regions on the crack surface are areas of heavy corrosion products. The crack initially propagated in a tunneled crack front configuration and first penetrated one surface (upper side surface in Figure 10) and later penetrated the other side surface thus forming the final curved crack front. Prior to opening the crack and examining the crack surface shown in Figure 10, a metallographic cross-section was performed normal to the crack to determine the microstructural crack path (this is the reason why two pieces are present in Figure 10). Figure 11a shows the location of the crack and the surrounding etched grain structure. Figures 11b and 11c show portions of the crack at higher magnification. Figure 11b shows that the cracking is intergranular and some regions exhibit extensive intergranular crack branching. Figure 11c shows the crack-tip region located on or very near a grain boundary.

Figure 12 shows the location of cracks found in the C5A forging top cap center region. Cracks were observed in fastener holes #349, #382, #380, #378, #376, #374 and #368. Figure 13 shows the surface of the crack that initiated at the mid-thickness region in fastener hole #382. The crack grew approximately 50 mm (2 inch) into a forging web and also terminated in fastener hole #349. The discolored regions on the crack surface are areas of heavy corrosion products. Figure 14 shows the conjugate surfaces of the crack that initiated on the opposite side of hole #382 near the mid-thickness region. The crack surface exhibits discoloration (corrosion products) along the edges (side surface regions) of the crack. Figure 15 shows the conjugate surfaces of the cracks that propagated between fastener holes #378 and #380. Here, the crack surface exhibits regions of distinct elevation change suggesting the initiation and growth of multiple cracks and crack coalescence. Because of the rather featureless crack surface, the site(s) of crack initiation were not identified. Figure 16 shows the conjugate surfaces of the crack that initiated at the mid-thickness of fastener hole #378. The dashed line marks the location of the curved final crack front. Figure 17 shows the conjugate surfaces of the crack that initiated at the mid-thickness of fastener hole #376. The dashed line marks the location of the curved final crack front. Regions of corrosion products (discoloration) are located near the final crack front. Figure 18 shows the conjugate surfaces of the crack that initiated at the mid-thickness of fastener hole #374. The dashed lines mark the location of the crack front; a portion of the crack front was unintentionally cut off during removal of the crack from the forging. Figure 19 shows the mating surfaces of the crack that initiated at fastener hole #368. The crack front region was cut off during removal of the specimen from the forging. The ridge along the middle of the crack surface suggests that two cracks nucleated and coalesced forming the ridge. The crack surface exhibits few features that could be used to identify the region of crack initiation in fastener hole #368. Figure 20 shows the crack that initiated from the opposite surface of fastener hole #368. The crack front region was cut off during removal of the specimen from the forging. The crack surface exhibits few features of interest.

Detailed scanning electron microscopy (SEM) was performed on most crack surfaces removed from the C5A forging. The SEM examinations revealed heavy corrosion products covered the surface of most cracks. EDS of the corrosion products revealed no unusual crack surface contaminant. Upon completion of all initial crack surface examinations, selected crack surfaces were cleaned with concentrated nitric acid (Unpublished research at NASA Langley Research Center has shown that a concentrated nitric acid cleaning procedure of aluminum crack surfaces removes surface oxides without disturbing the crack surface features). High magnification SEM examination of the cleaned crack surfaces revealed no features indicative of fatigue crack growth (striations) on cracks removed from the C5A tie box forging.

Fatigue Crack Growth Test Results

Detailed destructive examinations revealed a total of thirteen cracks in the C5A tie box forging and no cracking in the C5B forging. Table 1 summarizes the location and the number of cracks found in the C5A forging. The top cap center region exhibited the greatest amount of cracking followed by the top and bottom cap arm regions, respectively. The largest crack, 24 cm (9.5 inch) in length, was located in the top cap arm region.

The fatigue crack growth (FCG) characteristics of the C5A forging material exposed to room temperature laboratory air are shown in Figure 21. The plot of d*a*/dN versus ΔK shows the results of three FCG tests conducted using 30.5 mm wide C(T) specimens machined from the tie-box forging arm region shown in Figure 9. The specimen orientation was such that fatigue crack propagation was in the identical direction as the cracking observed in the forging arm region. Three FCG tests were conducted in laboratory air (relative humidity (RH) was not controlled or measured - the laboratory RH could range between 30 and 60%); one constant R = 0.05 test and two constant K_{max} tests at K_{max} = 13.2 MPa$\sqrt{m}$ (12.0 ksi$\sqrt{in}$) and K_{max} = 6.6 MPa$\sqrt{m}$ (6.0 ksi$\sqrt{in}$) were performed. During the constant K_{max} = 13.2 MPa$\sqrt{m}$ test (square symbols), the applied stress ratio was high, ranging from 0.7 to 0.9, and FCG rates (d*a*/dN) were not influenced by closure effects. For the K_{max} = 6.6 MPa$\sqrt{m}$ test (circle symbols), the applied stress ratio varied between R = 0.1 and R = 0.9; here, high R closure-free fatigue crack growth rates were identical to that observed during the high R constant K_{max} = 13.2 MPa$\sqrt{m}$ test. Region A shown in Figure 21 identifies the data produced at low stress ratio; here, lower R fatigue crack growth rates (circle symbols) are reduced compared to the high R data (square symbols). At the R = 0.1 d*a*/dN converges to closure effected d*a*/dN produced during the constant R = 0.05 test (triangle symbol). The FCG region designated region A was likely influenced by crack closure resulting in decreased d*a*/dN compared to the high R constant K_{max} FCG results. Respectively, the dotted and dashed lines shown in Figure 21 identify those data that represent the intrinsic (closure-free) and extrinsic (closure-affected) fatigue crack growth characteristics of the C5A 7075 forging. It is important to note that the intrinsic fatigue crack growth characteristics reveal that crack growth continued at extremely low crack-tip stress intensities (< 0.8 MPa$\sqrt{m}$). At constant R = 0.05, the unstable crack growth rate data reveal an apparent toughness $K_{app} \approx$ 16.5 MPa$\sqrt{m}$ (15.0 ksi$\sqrt{in}$).

Optical microscopy was conducted on the specimens after fatigue crack growth testing. The side surface of the FCG specimen tested at a K_{max} = 6.6 MPa$\sqrt{m}$ was polished and etched prior to FCG testing so that the path of the fatigue crack could be tracked relative to the microstructure. Figure 22a shows that the path of both the main crack and crack branching (upper arrows) are intergranular. Figure 22b shows the fatigue crack-tip region and reveals that the crack-tip is located along a grain boundary. These result show that the crack paths of fatigue cracks grown in laboratory air are along grain boundaries and exhibit intergranular crack branching similar to the cracks found in the C5A forging shown in Figure 11. Detailed SEM examination of the intergranular fatigue crack surfaces at high magnification showed that the surface morphology was similar to crack surfaces removed from the tie box forging. Similar to the forging cracks, no evidence of striations was observed on the fatigue test crack surfaces.

Stress Corrosion Cracking (SCC) Test Results

Stress corrosion cracking tests were performed in >95% relative humidity air using specimens machined from the C5A component. The data are plotted as d*a*/dt versus applied stress-intensity factor (K) in Figure 23 (solid circular symbols). Here, the applied K varied between 10 and 14.5 MPa$\sqrt{m}$. Because average crack growth rates are plotted in Figure 23, bars have been placed on each data point to represent the maximum and minimum rates observed during the time interval for which the average crack

growth rate was calculated. For comparison, SCC results for AA7075-T651 exposed to 100% relative humidity air [4] are also shown in Figure 23 (solid line). The comparison reveals that the C5A forging material exhibited accelerated SCC growth rates, by a factor of 2 to 4 as compared to the 7075-T651 plate alloy. The dashed line shown in Figure 23 represents the "upper bound" of the C5A data; here, the dashed curve has been given the same general shape as the 7075 plate SCC results and has been arbitrarily drawn though the upper most forging SCC data. Using the "upper bound" curve, a K_{ISCC} = 6 MPa$\sqrt{m}$ was estimated for the C5A forging alloy.

Fracture Toughness Test Results

The fracture toughness test results shown in Table 2 for specimens machined from both the C5A and C5B tie box forgings revealed that the C5A forging exhibited a toughness 26% lower than the C5B forging. The average fracture toughness for the four C5A tests is 17.5 MPa$\sqrt{m}$ and the average toughness for the three C5B tests was 23.8 MPa$\sqrt{m}$. Literature data for 7075-T651 plate suggest a toughness range from 25 MPa$\sqrt{m}$ for the transverse-longitudinal (T-L) orientation to 19 MPa$\sqrt{m}$ for the short-longitudinal (S-L) orientation [5]. The microstructural crack path observed for the C5A tie box forging is likely similar to the plate S-L orientation. Both the C5A cracking and the low toughness plate S-L orientation are the result of a grain boundary influenced crack path. Further work would be required to understand why the C5A tie box fracture toughness is considerably lower than the C5B forging toughness. Possible causes for the difference in C5A and C5B forging toughness properties include different levels of residual stress and/or different grain boundary microstructures resulting during thermo-mechanical processing.

Residual Stress Effects

The tunneling behavior exhibited by most of the cracks found in the C5A forging is a likely result of surface compressive stress from peening. Both the C5A and C5B tie boxes were machined from large forgings followed by a surface peening process. The peening forms a relatively shallow compressive surface that mitigates crack nucleation. It is likely that the fastener holes contained in the forgings were drilled after the peening process. The combination of the surface compressive stress and fastener hole stress concentration resulted in crack nucleation at the fastener hole mid-thickness. As the crack continued to propagate, the surface compressive residual stress forced the crack to grow along the interior, thus forming a highly tunneled crack front. The destructive examination results (refer to Figure 8) showed that many cracks grew to depths equivalent to two and three thicknesses before the crack front reached the forging surface. Crack tunneling is problematic because it is difficult to detect tunneled crack growth by nondestructive methods and visual inspections are unable to detect these cracks until the crack has propagated through the surface.

Residual stress can have a profound affect on crack growth properties. Residual stress resulting from a forging process is normally found in large aluminum forgings. The magnitude and type (compressive and tensile) can either enhance or retard crack growth. As an example, the effect of forging residual stress was observed during the removal of cracks from the C5A forging; as the forging was being cut a number of cracks exhibited rapid crack growth (pop-in). The observed "pop-in" is an indication of tensile residual stress that was relieved during the cutting operation. These observations suggest that significant residual stress is contained in the C5A forging; this effect could lead to premature cracking.

Summary and Conclusions

A number of cracks exhibited a complex pattern of corrosion products suggesting the presence of a corrosive environment. Consistent with environmentally enhanced crack growth in alloy 7075, all cracks

found in the C5A tie box exhibited an intergranular path with regions of intergranular secondary cracking. Most cracks propagated with a highly tunneled crack front and a number of cracks grew to substantial lengths (equivalent to two and three thickness) before becoming through-the-thickness cracks. Surface peening followed by fastener hole drilling is a likely cause of the observed crack-tunneled configuration. As a result of this processing method, cracking was difficult to detect by visual and standard NDE inspection methods, and many cracks were not be detected until removal of the tie-box from the aircraft.

Laboratory testing revealed that the C5A forging exhibited material properties (fracture toughness, stress corrosion cracking and fatigue crack growth characteristics) that are not optimum. The C5A forging exhibited a fracture toughness that is 26% lower than the C5B tie box alloy. Stress corrosion cracking tests revealed that the C5A forging alloy is more susceptible to intergranular SCC than 7075-T6 plate. Fatigue crack growth tests showed that the C5A alloy exhibited rapid intergranular crack growth having a fatigue crack growth threshold of less than 0.8 $MPa\sqrt{m}$.

A variety of factors, including reduced material properties, environment, and possibly unknown local stress, combined to cause multi-site cracking in the C5A forging. Test results that showed reduced fracture toughness, rapid intergranular fatigue crack growth, and increased SCC susceptibility suggest that forging thermo-mechanical processing produced a microstructure with an increased susceptibility for environmentally enhanced intergranular cracking. The tie box cracking was linked to an intergranular microstructure crack path that is somewhat analogous to cracking in the S-L plate orientation. The drilling of fastener holes resulted in exposed grain boundary microstructure ("end grain") along the surface; grain boundary microstructure is environmentally susceptible and exhibits low fracture properties. The exposed "end grains" likely acted as sites for cracking because of preferential corrosion and/or a local stress concentration. These metallurgical and environmental factors along with local loads (operational, fit-up and possible residual stresses) combined to cause multiple-site cracking.

The understanding of local loads is critical to determining the operational life of replacement C5A and existing C5B tie box forgings. Because local loads are unknown, it is impossible to determine whether SCC or an environmental fatigue crack growth mechanism caused cracking in the C5A tie box forging. Previous guidelines have suggested that stress corrosion cracking is the operative damage mechanism when environmentally induced intergranular cracks with secondary cracking are observed, no evidence of fatigue (striations) is detected and the direction of crack propagation ("directionality") is not perpendicular to the applied loading direction. Contrary to these SCC guidelines, intergranular cracks with secondary cracking, similar to that found in the C5A forging, were produced during laboratory air fatigue crack growth testing. Furthermore, detailed examination of the intergranular fatigue crack surfaces revealed no evidence of striated crack growth. Therefore, it is important to emphasize that intergranular cracking is not solely a sustained-load cracking mode; intergranular cracking with no evidence of striation can occur under fatigue loading. A true understanding of the local loading is required to determine the effect of "directionality" before the C5A tie box damage mechanism can be identified. This understanding is important because environmentally enhanced fatigue crack growth can occur at loads well below the threshold load for stress corrosion cracking, and thus have a profound affect on life.

References

1. J. E. Hatch, Editor. *Aluminum: Properties and Physical Metallurgy*, American Society for Metals, Metals Park, OH, 1984.

2. ASTM: Standard Test Method for Measurement of Fatigue Crack Growth Rates. *Annual Book of ASTM Standards, E 647-99,* 03.01, 2000, pp. 591-630.

3. ASTM: Standard Test Method for Measurement of Fatigue Crack Growth Rates. *Annual Book of ASTM Standards, E 399-90,* 03.01, 2000, pp. 431-461.

4. *Advances in Corrosion Science and Technology*, Vol.2, Mars G. Fontana and Roger W. Staehle, Eds., Plenum Press, New York, N.Y., p. 172 (1972).

Table 1. Summary of C5A Tie Box Destructive Examination

	Fastener Hole Location*	Number of Cracks
Top Cap Center Region	#349 to #382L, #382R, #380 to 378R, #376L, #376R, #374, #368L, #368R	8 Cracks
Top Cap Arm Region	#315 to #311, #383 to #385L, 385R to #387, #295	4 Cracks
Bottom Cap Arm Region	#276	1 Crack
* R and L denote cracking from the right or left side of the fastener hole.		

Table 2. Fracture toughness results for C5A and C5B material.

	C5A material K_{Ic} (MPa$\sqrt{m}$)	C5B material K_{Ic} (MPa$\sqrt{m}$)
	16.2	23.7
	17.4	24.2
	20.2	23.5
	16.3 *	
Average	17.5	23.8

* Fatigue pre-crack configuration did not meet ASTM E 399 requirements [3]. Variance from other test results is small, therefore, the test result is deemed reasonable for inclusion.

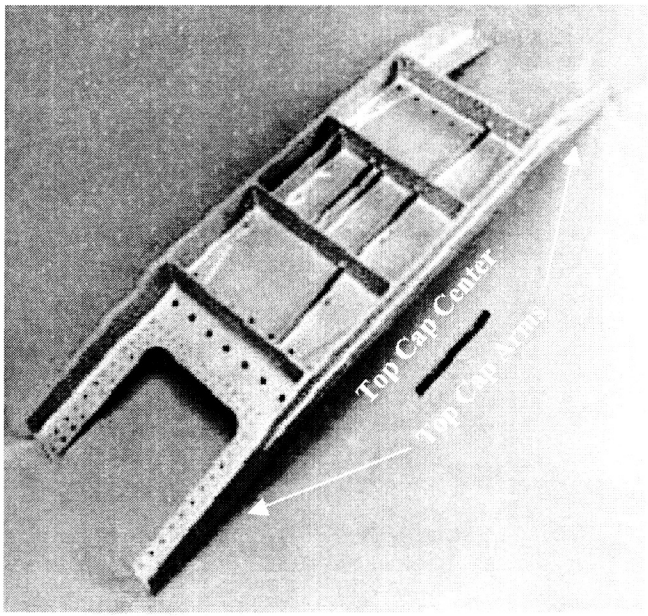

(a)

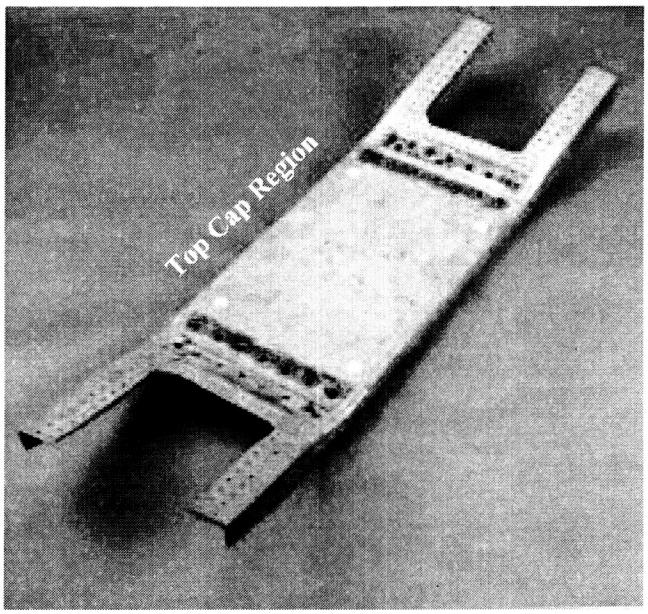

(b)

Figure 1. The photographs show the general features of the C5A tie box forging.

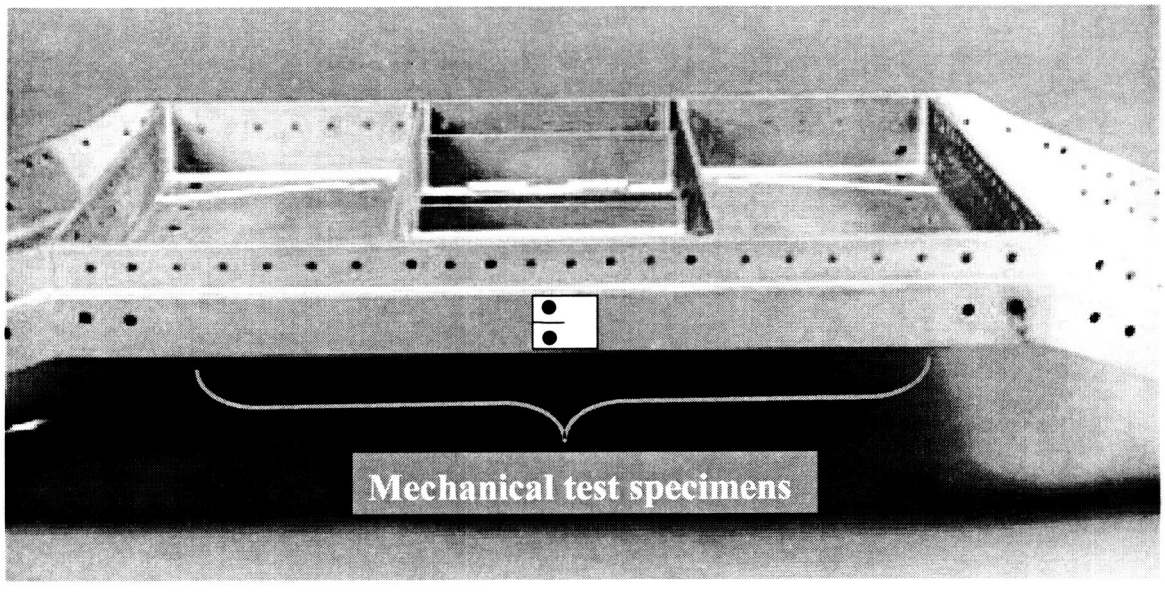

Figure 2. The photograph shows the C5A forging top cap center region. Fracture toughness and stress corrosion specimens were machined from the cap region for the C5A and C5B forging.

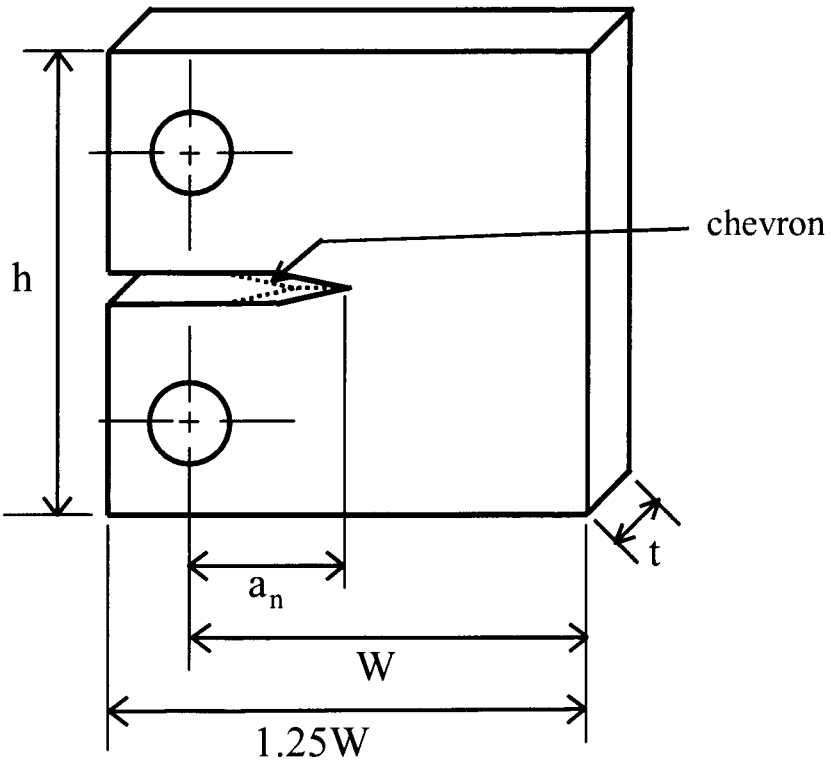

	C(T) FCGR	C(T) SCC	WOL Fracture
a_n (mm)	5.84	10.2	13.2
W (mm)	30.5	50.8	52.3
2h (mm)	36.6	61.0	50.8
t (mm)	6.35	12.7	22.9
chevron	no	yes (120°)	yes (120°)

Figure 3. The figure shows the general configuration and dimensions for C(T) and WOL specimens.

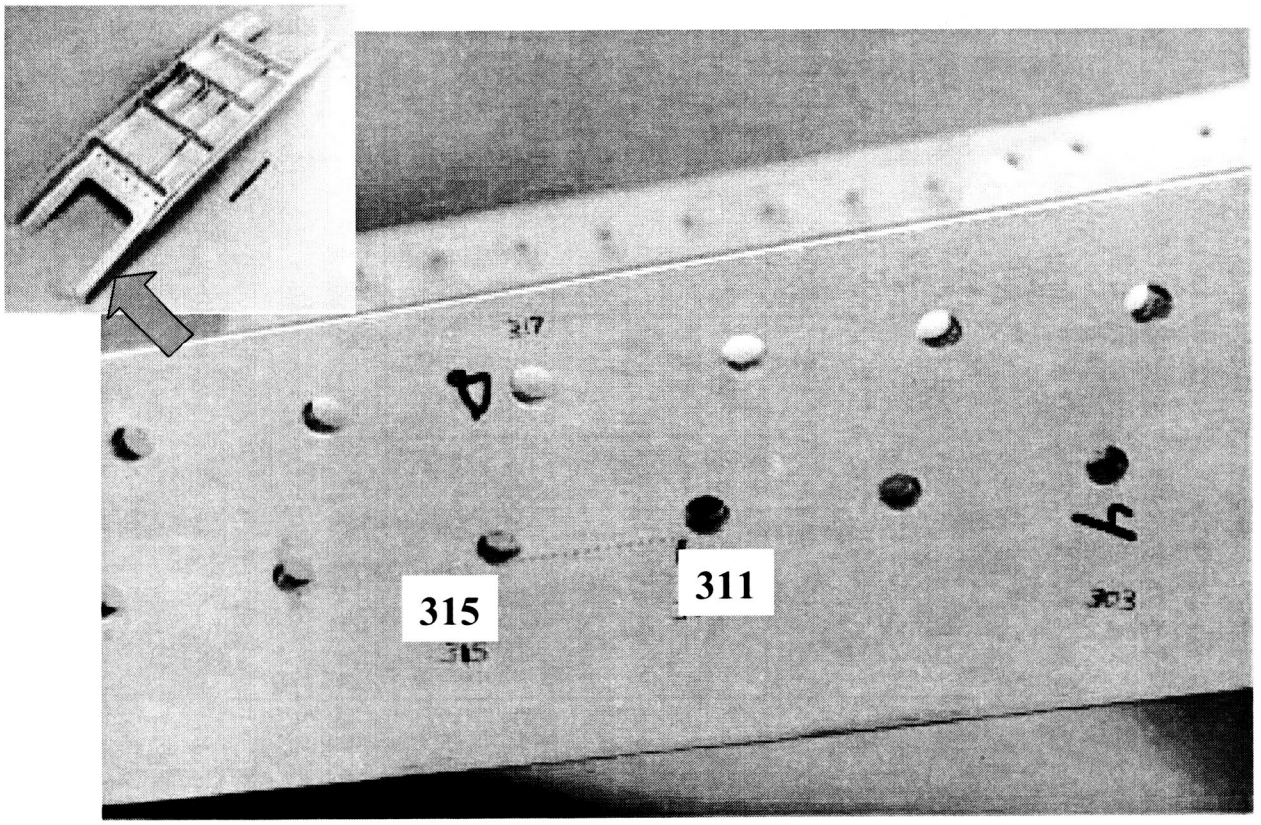

Figure 4. The large photograph shows the outside surface top cap arm region of the C5A tie-box (the region is identified by the arrow in the small photograph). A dashed line identifies the location of the crack between fastener holes #311 and #315.

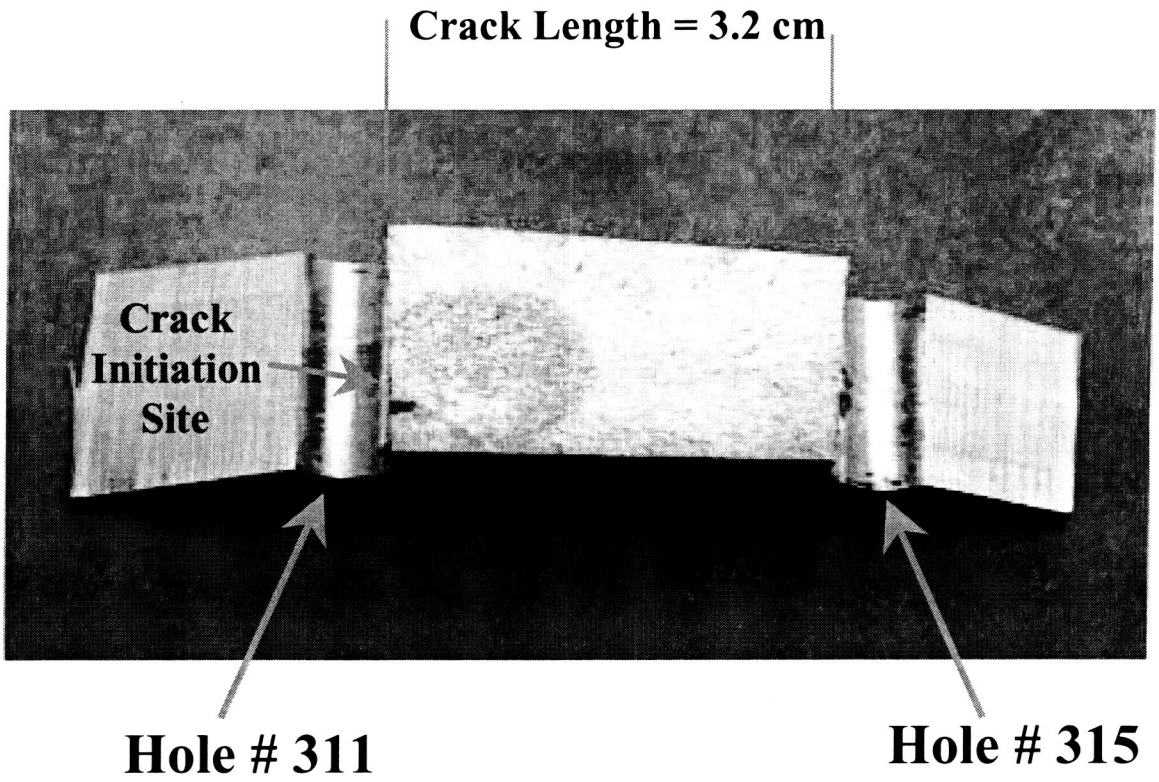

Figure 5. The photograph shows the surface of the crack emanating from hole #311 and propagating to hole #315.

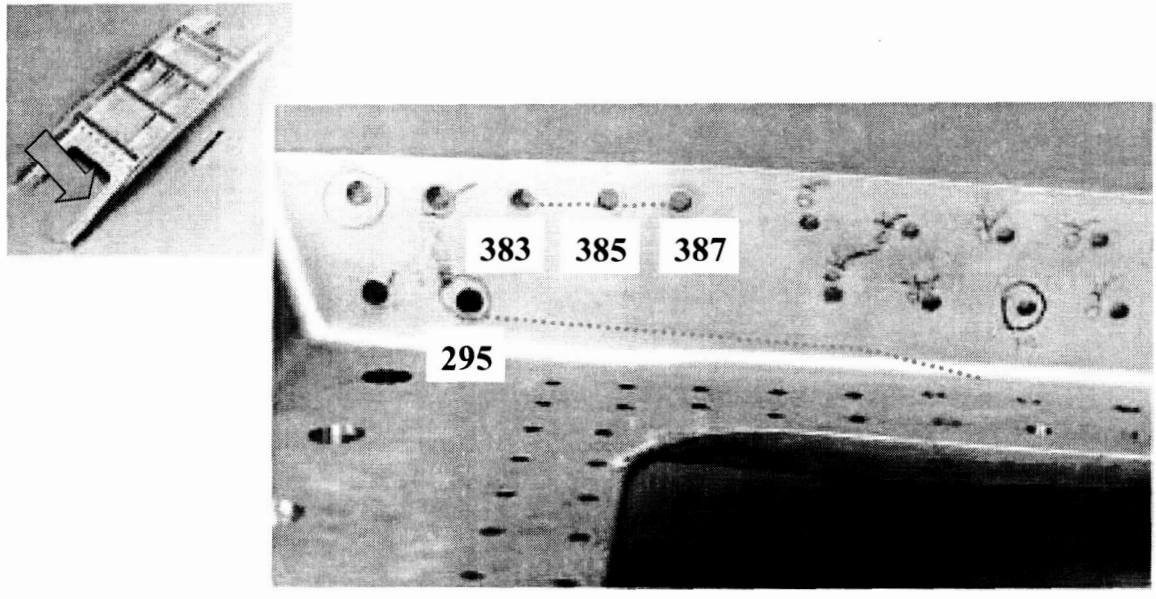

Figure 6. The large photograph shows the inside surface of the top cap arm region of the C5A tie-box (the region is identified by the arrow in the small photograph). Dashed lines identify the cracks at fastener holes #383, #385, #387 and #295.

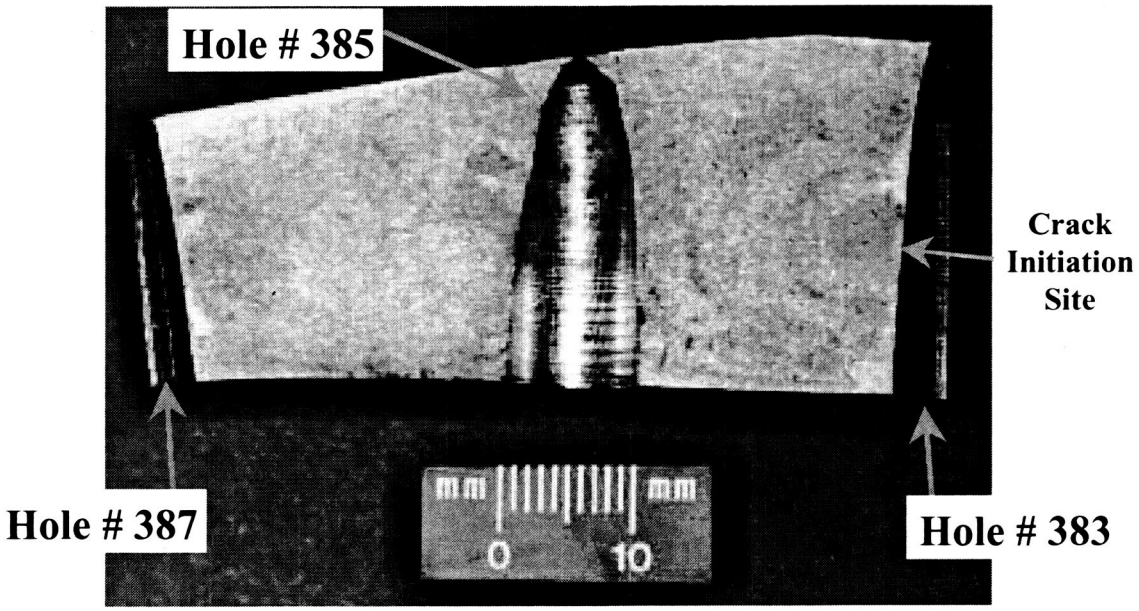

Figure 7. The photograph shows the surface of the crack that initiated from fastener hole #383 and terminating at hole #387.

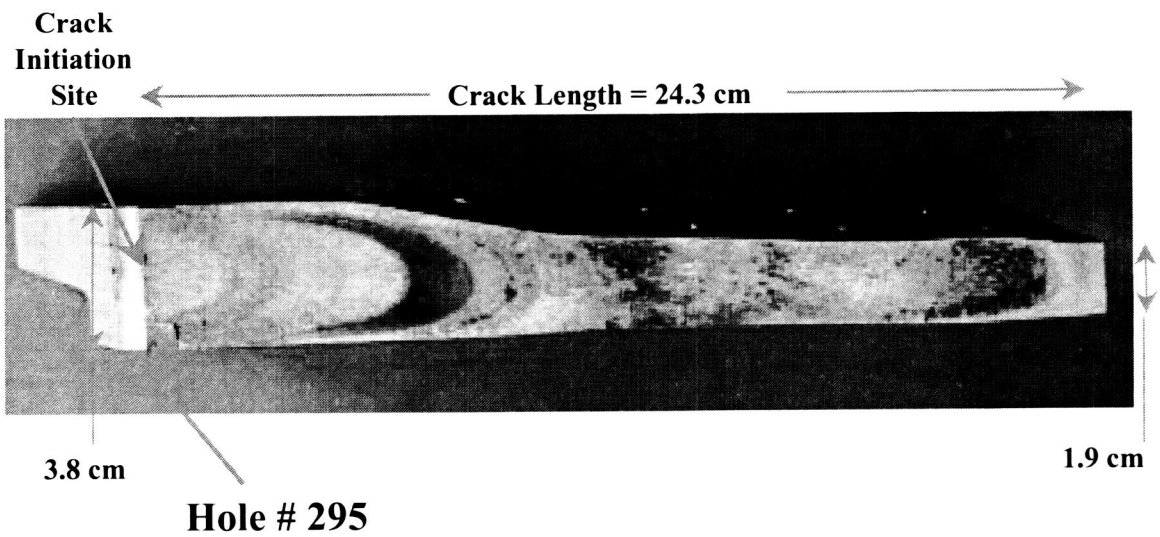

Figure 8. The photograph shows the surface of the crack emanating from fastener hole #295.

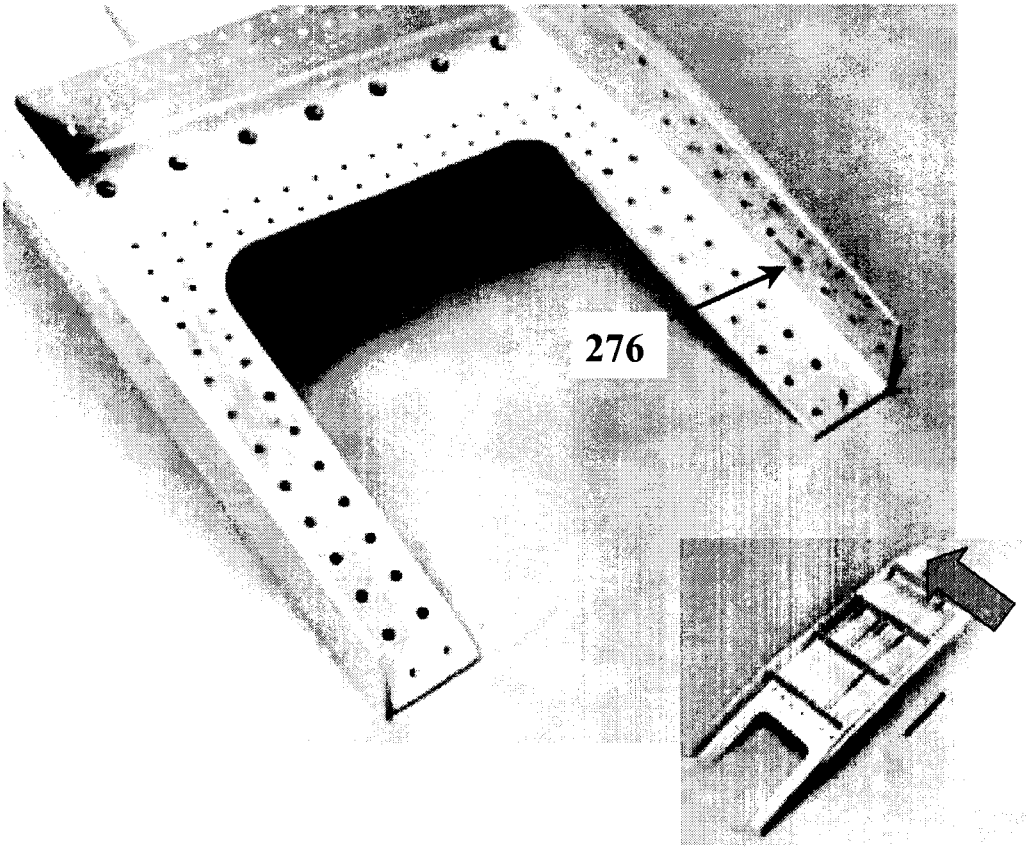

Figure 9. The large photograph shows the inside surface of the lower cap arm region of the C5A tie-box (the region is identified by the arrow in the small photograph). The line identifies the location of the crack at fastener hole #276.

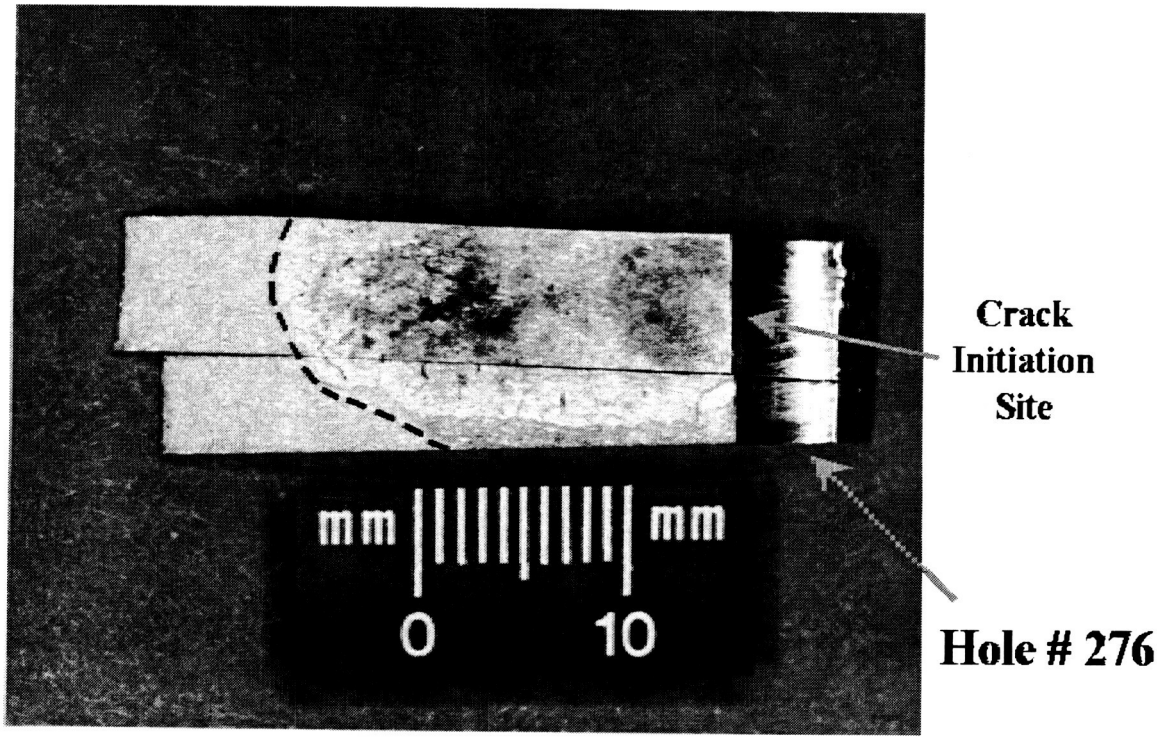

Figure 10. The photograph shows the surface of the crack that initiated at fastener hole #276.

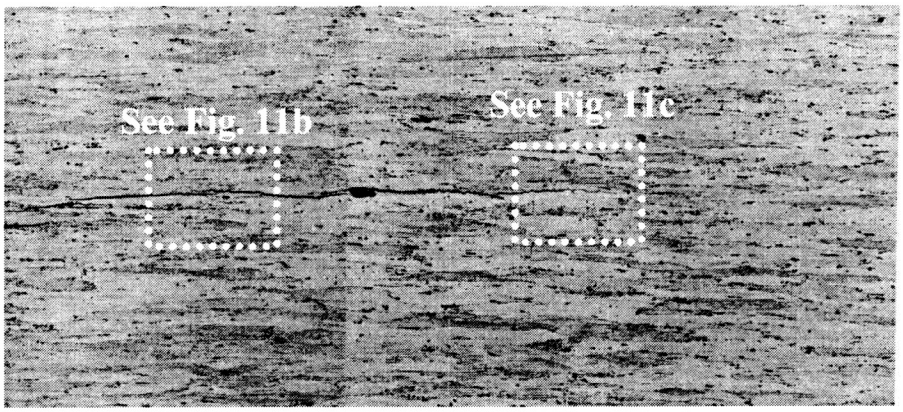

(a)

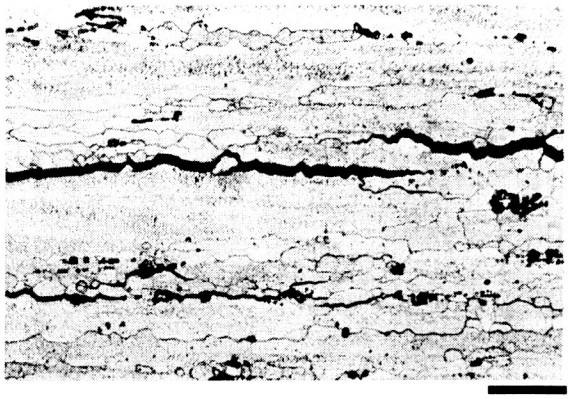

(b)

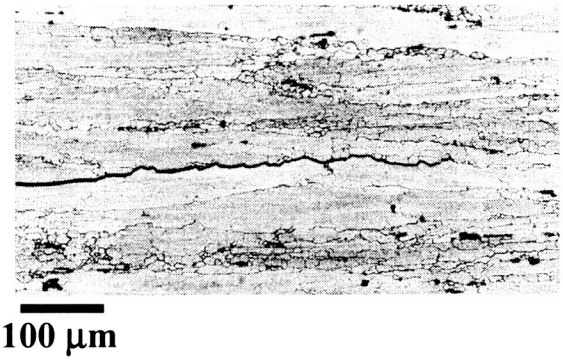

c)

Figure 11. Shown are optical micrographs of the crack emanating from fastener hole #276. The location of Figures 11b and 11c are identified (square regions) in Figure 11a.

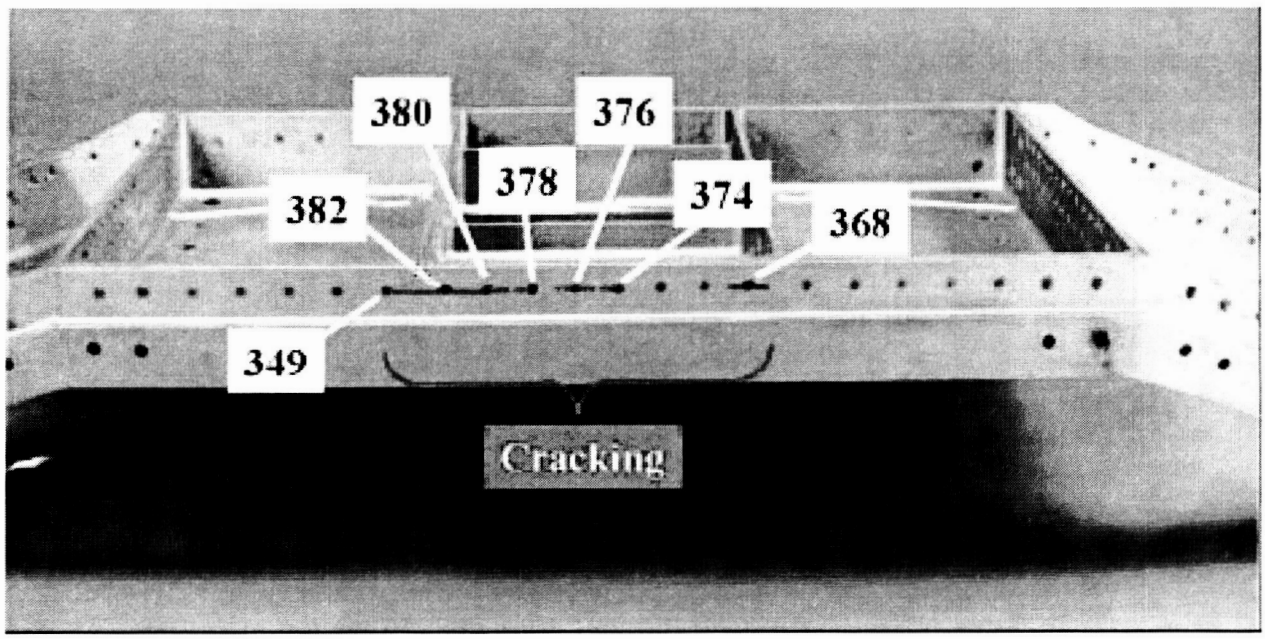

Figure 12. The photograph of C5A tie-box forging shows the location of cracking (red solid and dashed lines) in the top cap center region (fastener holes #349, #382, #380, #378, #376, #374 and #368).

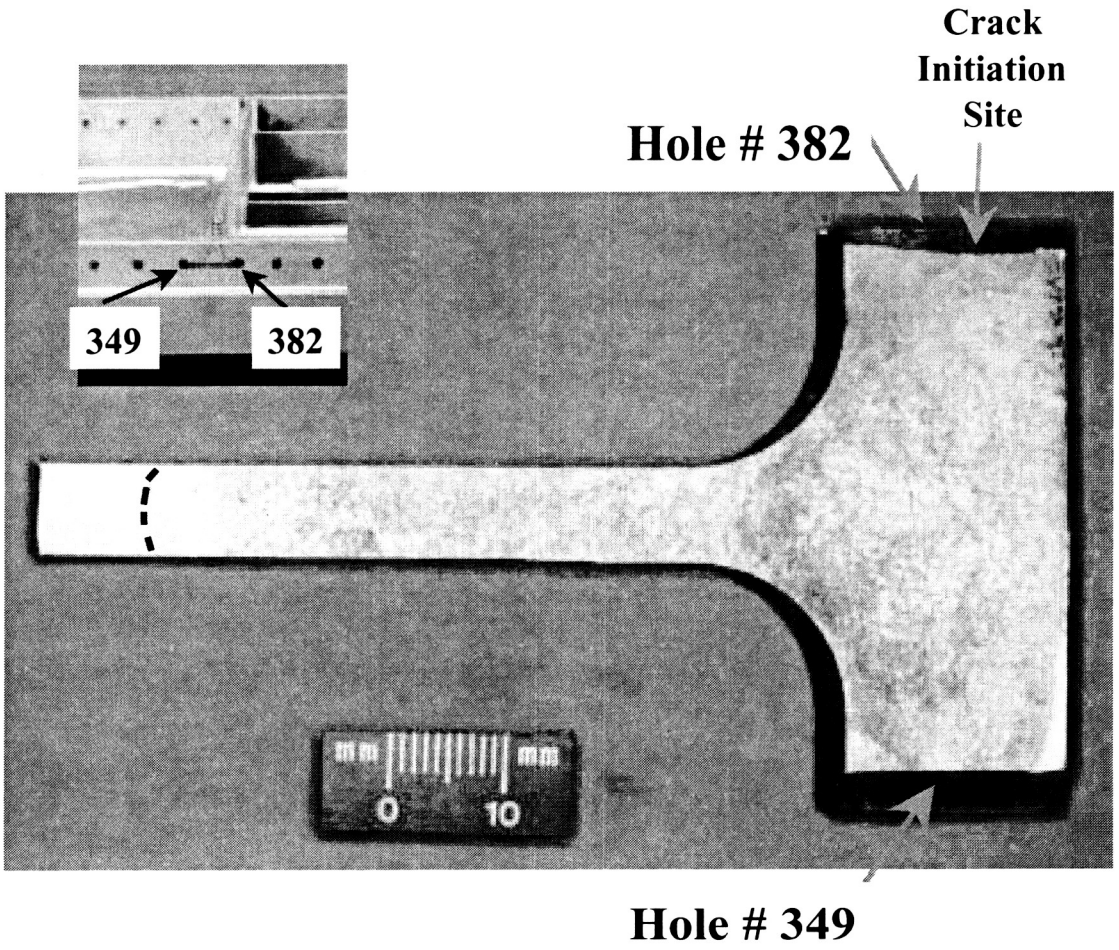

Figure 13. The photograph shows the surface of the crack emanating from fastener hole #382 and propagating into hole #349 and the forging web. The location of fastener holes #349 and #382 is shown in the small photograph. The dashed line shows the final crack front in the forging web.

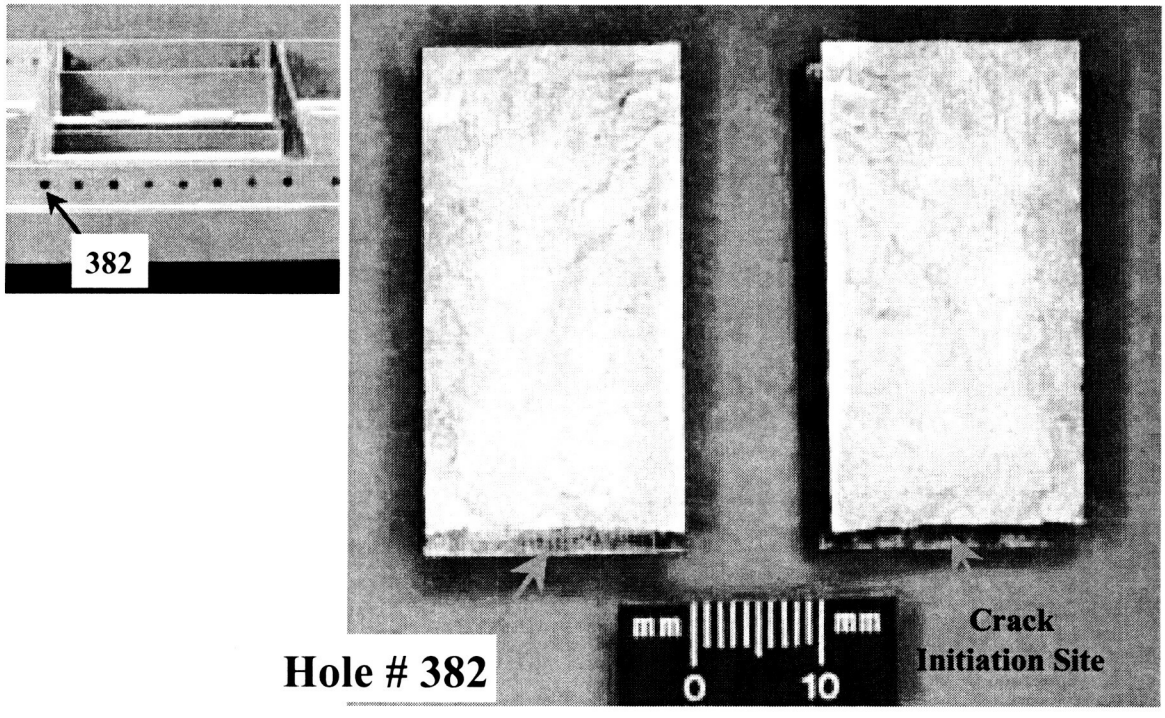

Figure 14. The photograph shows both surfaces of the crack emanating from fastener hole #382. The location of fastener hole # 382 is shown in the small photograph.

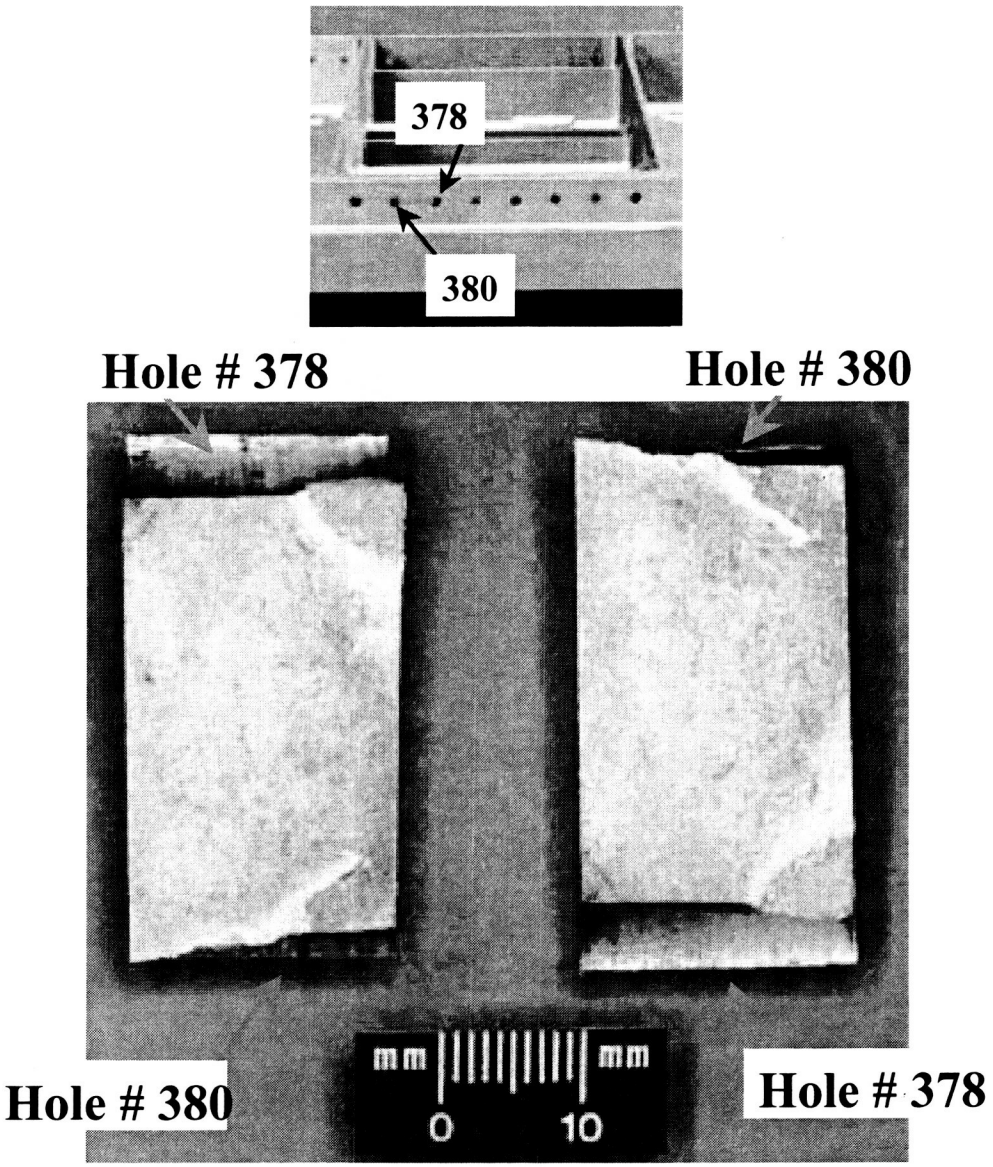

Figure 15. The photograph shows both surfaces of the crack located between fastener holes #380 and #378. The location of fastener holes #380 and #378 is shown in the small photograph.

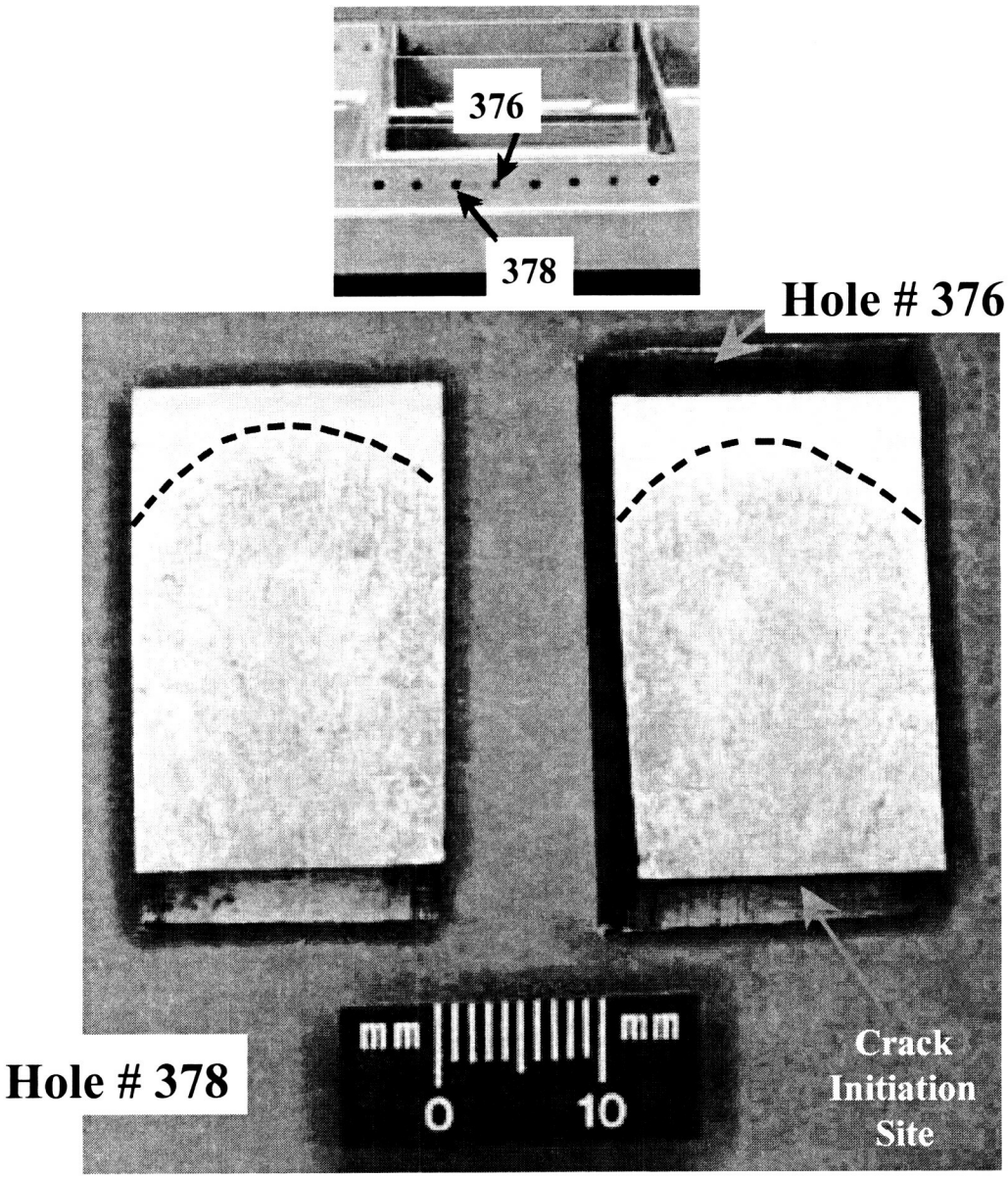

Figure 16. The photograph shows both surfaces of the crack emanating from fastener hole #378. The location of fastener holes #378 and #376 is shown in the small photograph.

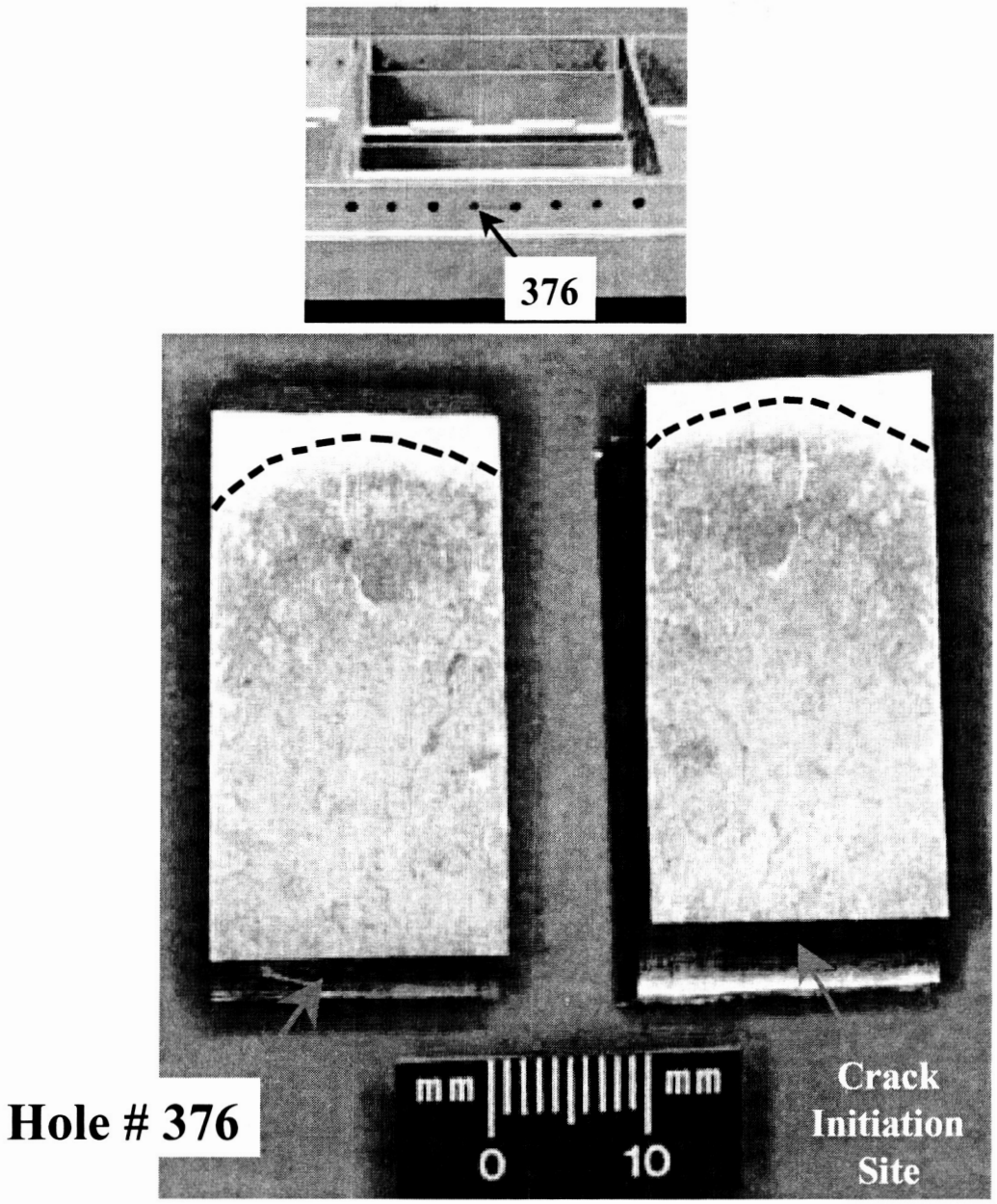

Figure 17. The photograph shows both surfaces of the crack emanating from fastener hole #376. The location of fastener hole #376 is shown in the small photograph.

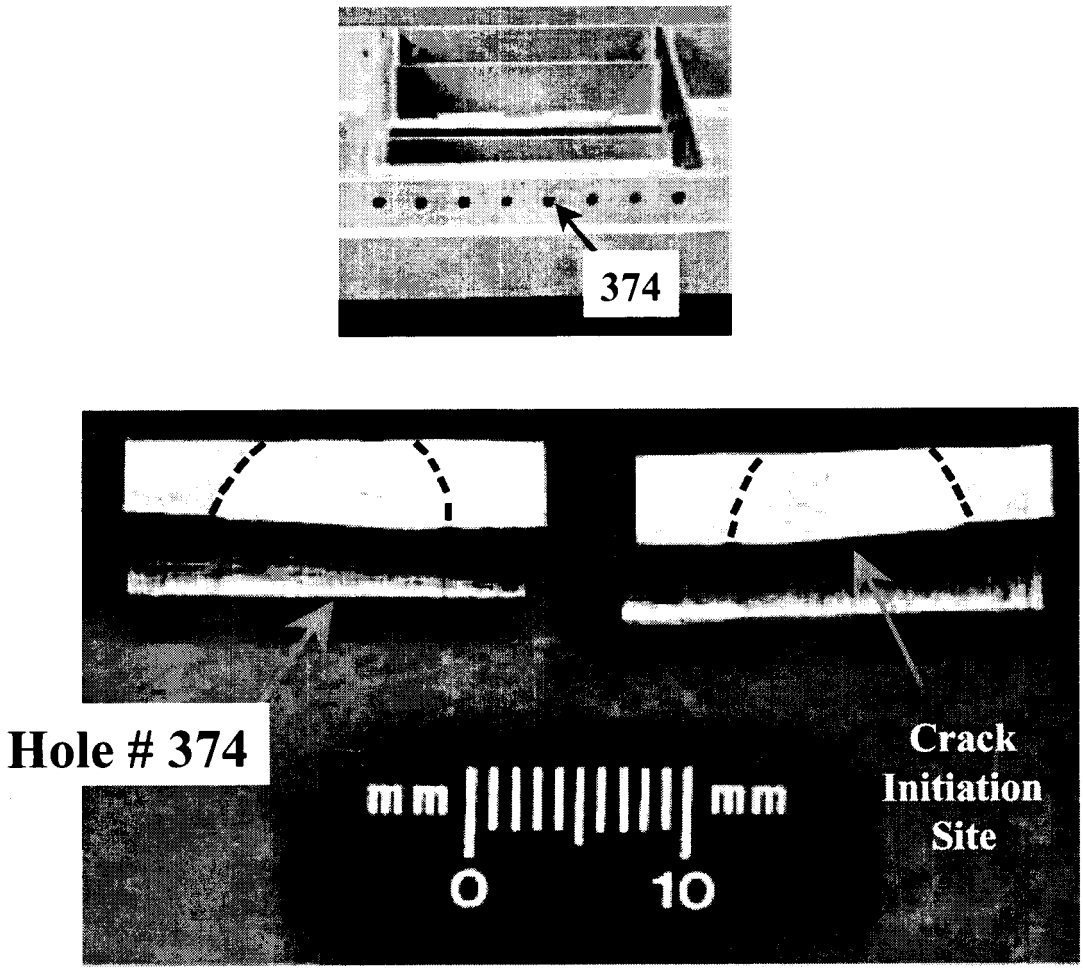

Figure 18. The photograph shows both surface of the crack emanating from fastener hole #374. The location of fastener hole #374 is shown in the small photograph.

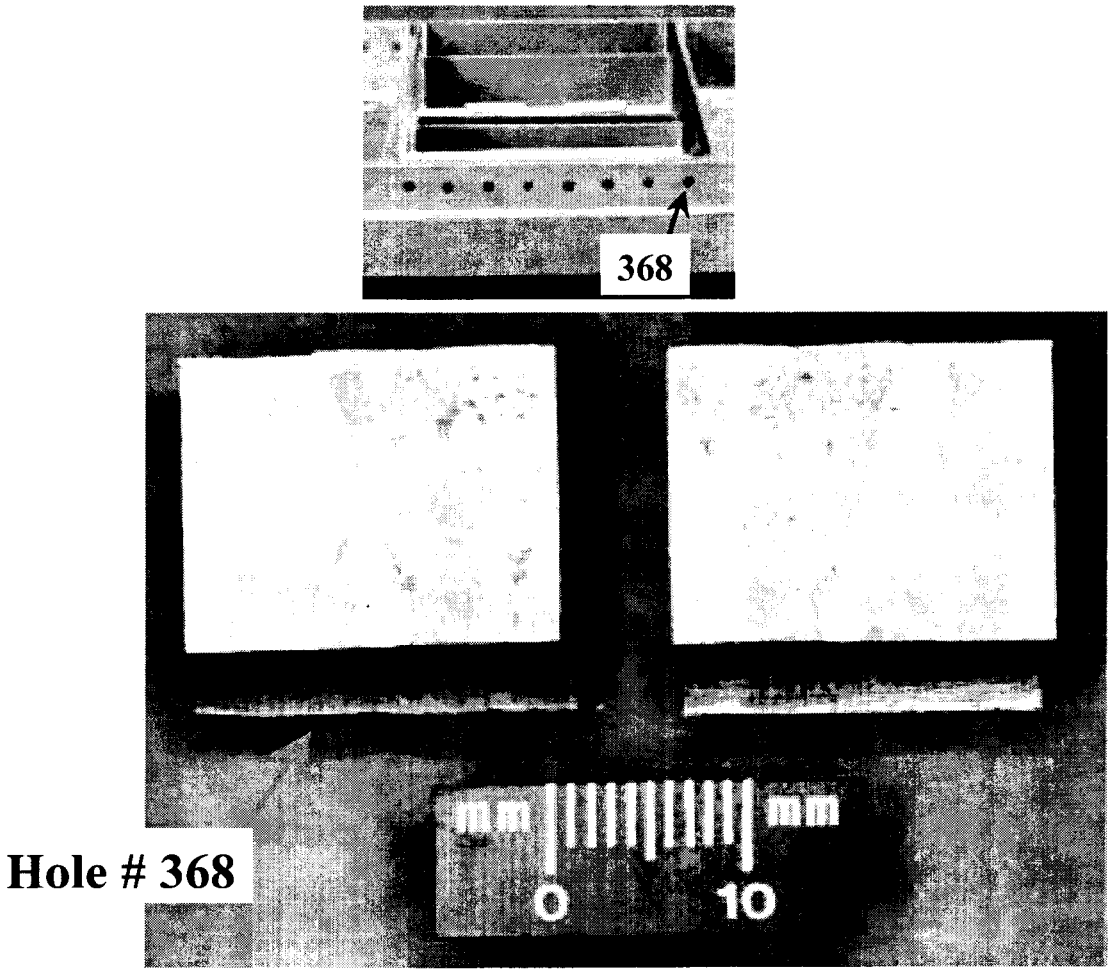

Figure 19. The photograph shows both surfaces of the crack emanating from fastener hole #368. The location of fastener hole #368 is shown in the small photograph.

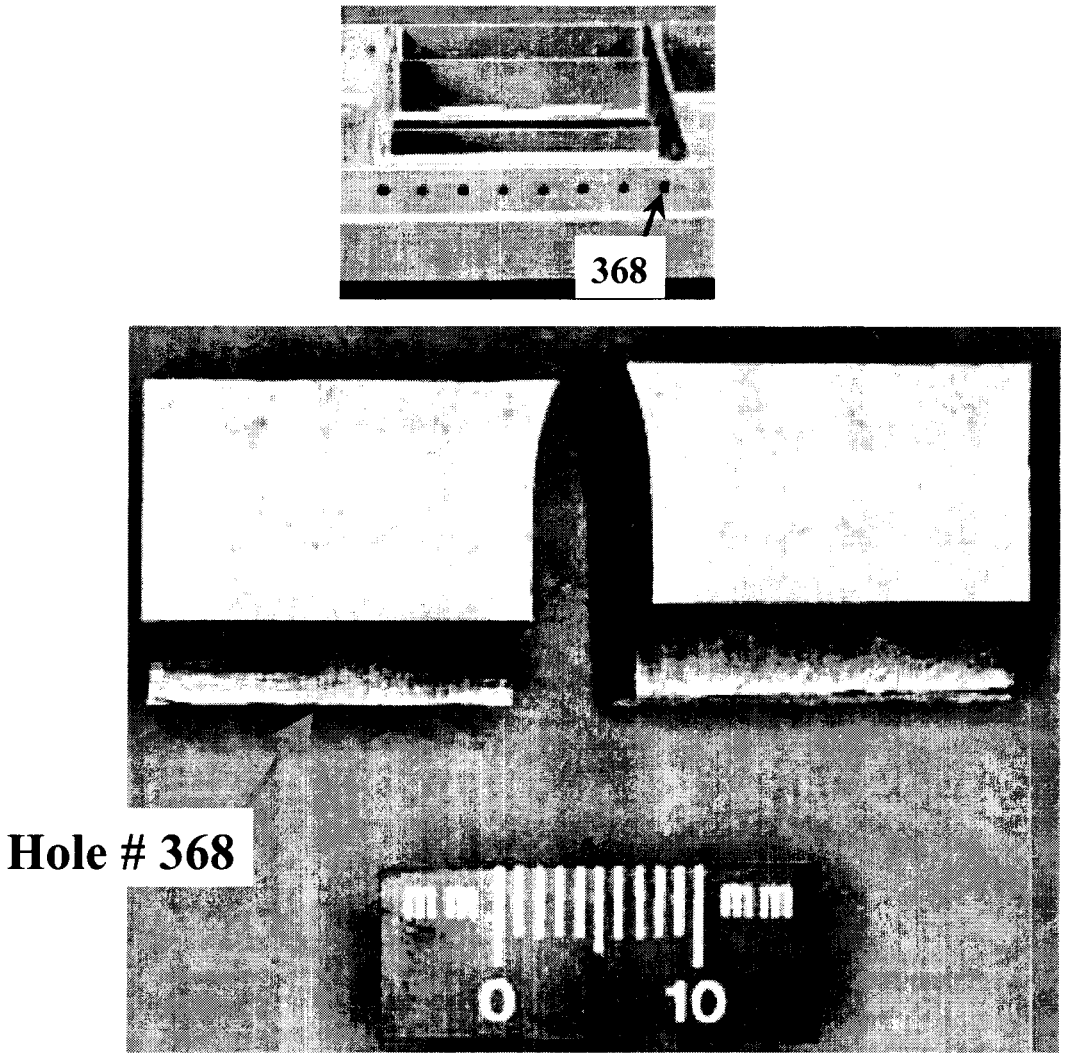

Figure 20. The photograph shows both surfaces of the crack emanating from fastener hole #368. The location of fastener hole #368 is shown in the small photograph.

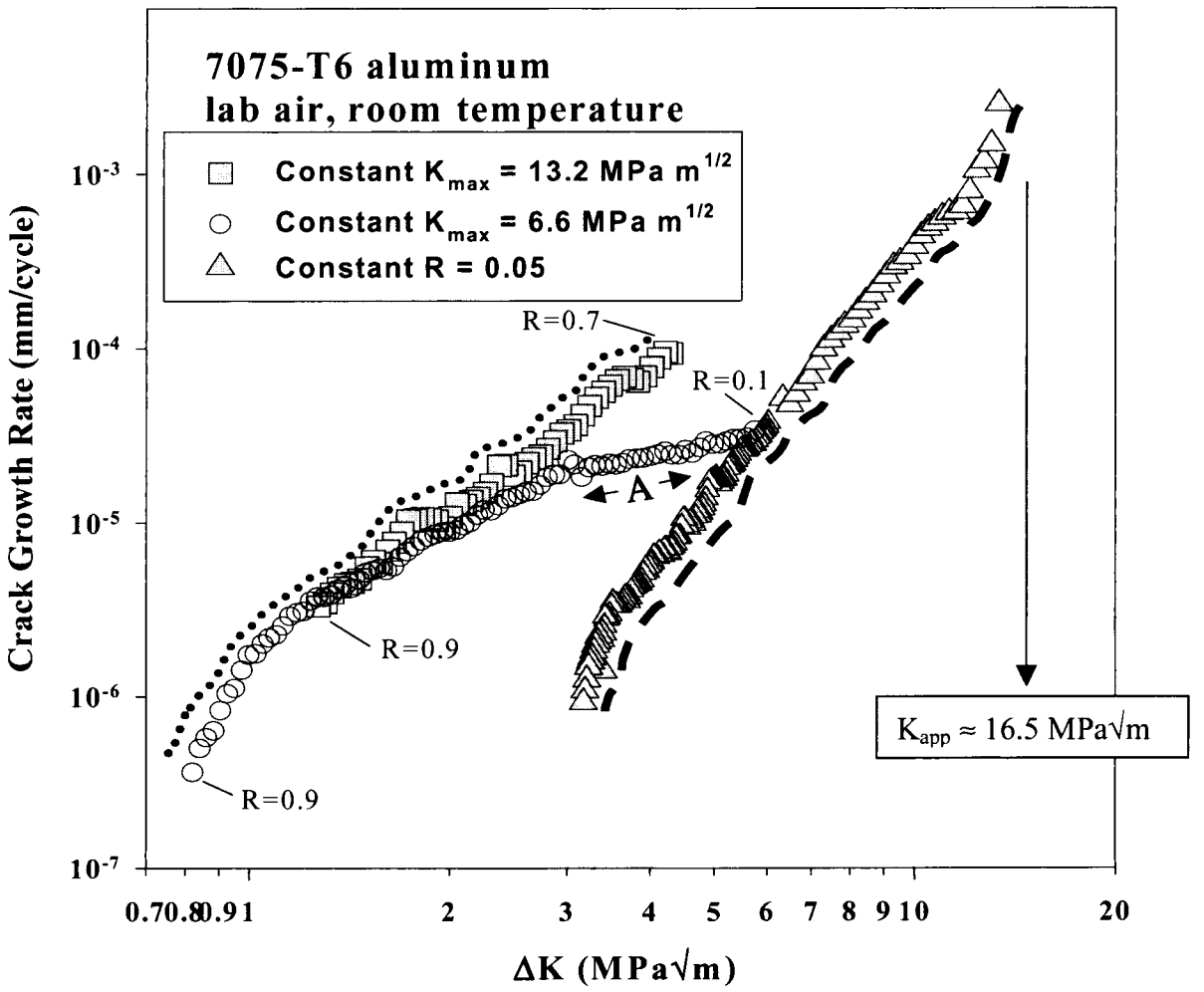

Figure 21. A plot shows the intrinsic (closure free) and extrinsic (closure affected) fatigue crack growth characteristics of the C5A tie box material.

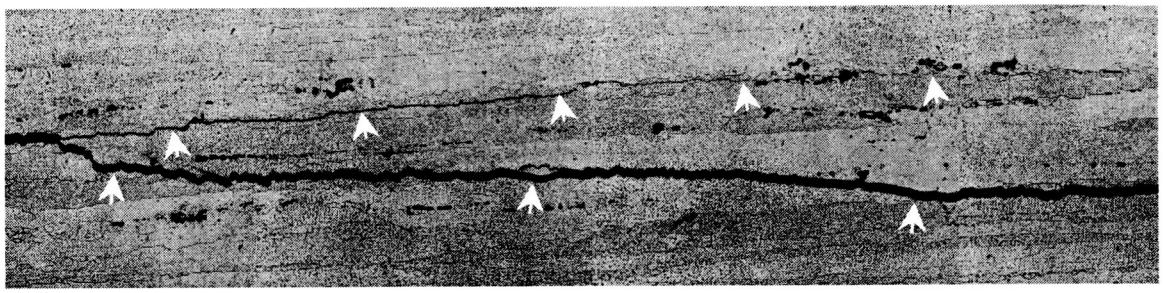

(a)

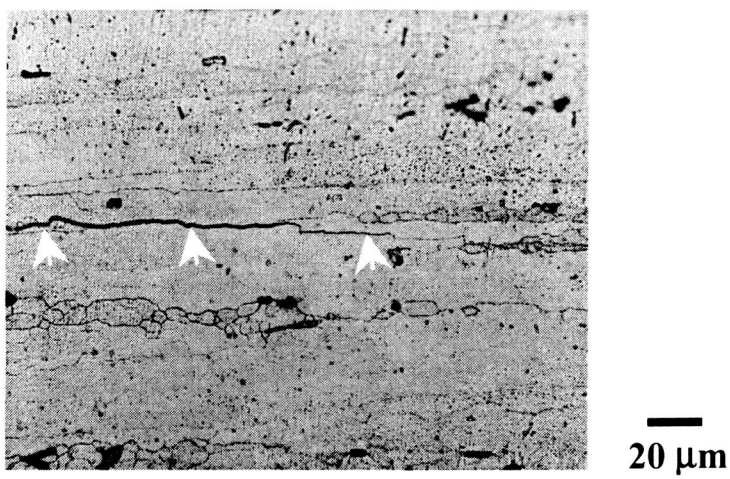

(b)

Figure 22. Optical micrographs of an etched surface showing the intergranular fatigue crack growth crack path for FCG test conducted on C5A material. (a) The micrograph shows the main fatigue crack (lower arrows) and a secondary fatigue crack (upper arrows) that propagated along or near grain boundaries. (b) The micrograph shows the fatigue crack tip region (marked by arrows) and definitively shows that the fatigue propagated along grain boundaries.

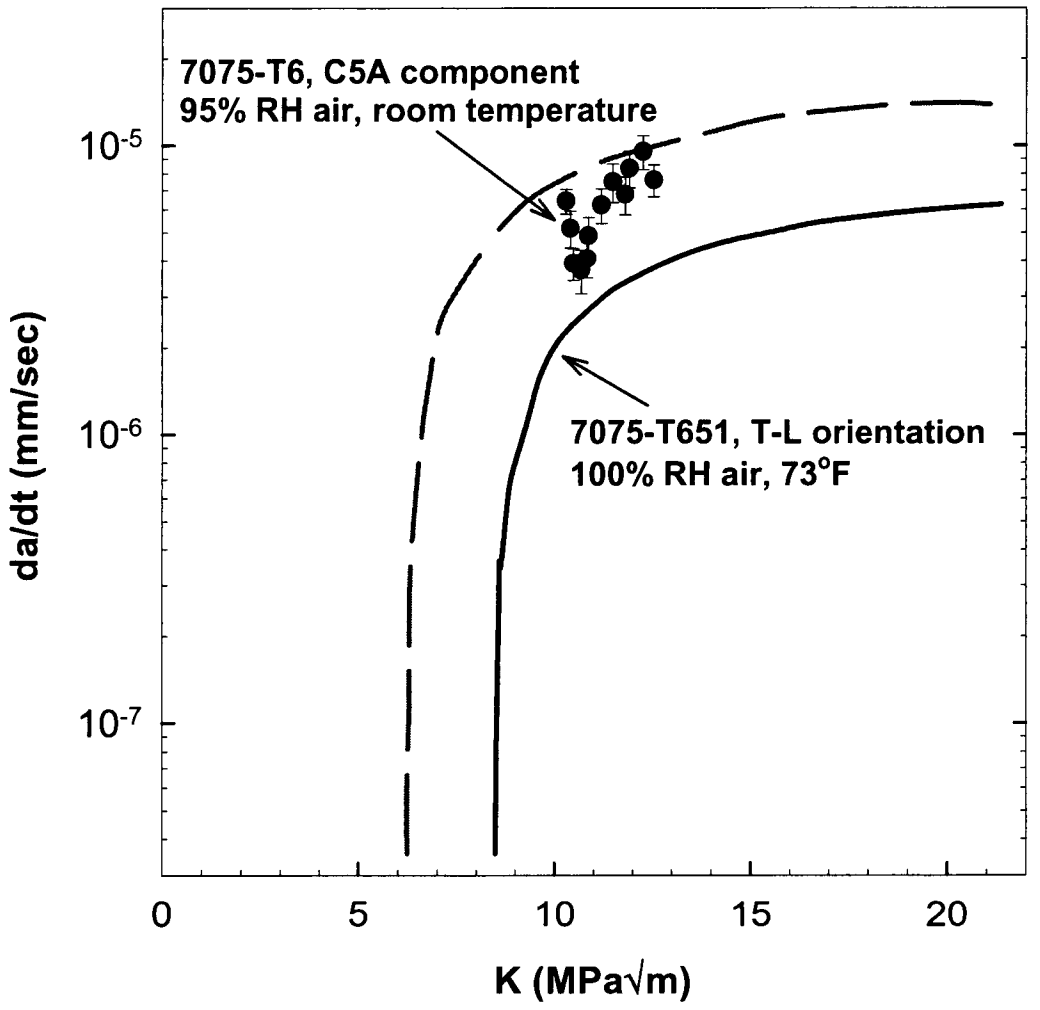

Figure 23. The plot shows the stress corrosion cracking characteristics of C5A tie box material in 95% relative humidity air.

REPORT DOCUMENTATION PAGE

Form Approved
OMB No. 0704-0188

1. AGENCY USE ONLY (*Leave blank*)	2. REPORT DATE	3. REPORT TYPE AND DATES COVERED
	August 2003	Technical Memorandum

4. TITLE AND SUBTITLE
Characterization of Cracking and Crack Growth Properties of the C5A Aircraft Tie-Box Forging

5. FUNDING NUMBERS
706-62-31-51

6. AUTHOR(S)
Robert S. Piascik, Stephen W. Smith, John A. Newman, and Scott A. Willard

7. PERFORMING ORGANIZATION NAME(S) AND ADDRESS(ES)
NASA Langley Research Center
Hampton, VA 23681-2199

U.S. Army Research Laboratory
Vehicle Technology Directorate
NASA Langley Research Center
Hampton, VA 23681-2199

8. PERFORMING ORGANIZATION REPORT NUMBER
L-18309

9. SPONSORING/MONITORING AGENCY NAME(S) AND ADDRESS(ES)
National Aeronautics and Space Administration
Washington, DC 20546-0001
and
U.S. Army Research Laboratory
Adelphi, MD 20783-1145

10. SPONSORING/MONITORING AGENCY REPORT NUMBER
NASA/TM-2003-212439
ARL-TR-3046

11. SUPPLEMENTARY NOTES

12a. DISTRIBUTION/AVAILABILITY STATEMENT
Unclassified-Unlimited
Subject Category 26 Distribution: Nonstandard
Availability: NASA CASI (301) 621-0390

12b. DISTRIBUTION CODE

13. ABSTRACT (*Maximum 200 words*)
Detailed destructive examinations were conducted to characterize the integrity and material properties of two aluminum alloy (7075-T6) horizontal stabilizer tie box forgings removed from U.S. Air Force C5A and C5B transport aircraft. The C5B tie box forging was found to contain no evidence of cracking. Thirteen cracks were found in the C5A forging. All but one of the cracks observed in the C5A component were located along the top cap region (one crack was located in the bottom cap region). The cracks in the C5A component initiated at fastener holes and propagated along a highly tunneled intergranular crack path. The tie box forging fatigue crack growth, fracture and stress corrosion cracking (SCC) properties were characterized. Reported herein are the results of laboratory air fatigue crack growth tests and 95% relative humidity SCC tests conducted using specimens machined from the C5A forging. SCC test results revealed that the C5A forging material was susceptible to intergranular environmental assisted cracking: the C5A forging material exhibited a SCC crack-tip stress-intensity factor threshold of less than 6 MPa$\sqrt{m}$. Fracture toughness tests revealed that the C5A forging material exhibited a fracture toughness that was 25% less than the C5B forging. Because both fatigue crack propagation and SCC exhibit similar intergranular crack path behavior, the damage mechanism resulting in multi-site cracking of tie box forgings cannot be determined unless local cyclic stresses can be quantified.

14. SUBJECT TERMS
corrosion fatigue; stress corrosion cracking; aluminum alloys

15. NUMBER OF PAGES
36

16. PRICE CODE

17. SECURITY CLASSIFICATION OF REPORT	18. SECURITY CLASSIFICATION OF THIS PAGE	19. SECURITY CLASSIFICATION OF ABSTRACT	20. LIMITATION OF ABSTRACT
Unclassified	Unclassified	Unclassified	UL